

# A phenomenological multiband Eliashberg model for LiFeAs

G A Ummarino<sup>1</sup>, Sara Galasso<sup>1</sup> and A Sanna<sup>2</sup>

<sup>1</sup> Istituto di Ingegneria e Fisica dei Materiali, Dipartimento di Scienza Applicata e Tecnologia, Politecnico di Torino, Corso Duca degli Abruzzi 24, I-10129 Torino, Italy

<sup>2</sup> Max-Planck-Institut für Mikrostrukturphysik, Weinberg 2, D-06120 Halle, Germany

E-mail: [giovanni.ummarino@infm.polito.it](mailto:giovanni.ummarino@infm.polito.it)

Received 20 February 2013, in final form 28 March 2013

Published 25 April 2013

Online at [stacks.iop.org/JPhysCM/25/205701](http://stacks.iop.org/JPhysCM/25/205701)

## Abstract

The phenomenology of a LiFeAs superconductor can be explained in the framework of four-band  $s_{\pm}$ -wave Eliashberg theory. We have examined the experimental data available in the literature and we have found that it is possible to reproduce the experimental critical temperature, the gap values and the upper critical magnetic field within an effective model in a moderately strong coupling regime that must include both an intraband term  $\lambda_{11} \sim 0.9$  and an interband spin-fluctuation ( $\lambda_{\text{tot}}^{\text{sf}} \sim 1.5$ ) coupling. The presence of a nonnegligible intraband coupling can be a fictitious effect of the violation of Migdal's theorem.

(Some figures may appear in colour only in the online journal)

The family of iron pnictide superconductors, discovered by the Hosono group [1] in 2008, has been the focus of intense research over the last four years. Many compounds with different crystal structures and physical properties have been discovered and characterized [2–4], among them LiFeAs [5] has proved to be a peculiar one.

First of all, LiFeAs, unlike almost all other iron-compounds, does not need either charge doping or pressure to condense in the superconducting state [5]. This implies that no disorder is present. Further, it does not seem to be magnetic and angle-resolved photoemission spectroscopy (ARPES) reports poor nesting [6]. At a glance these characteristics could turn us away from the idea of an unconventional pairing mechanism, however the phonon-mediated coupling seems to be too weak [7] to explain the relatively high critical temperature ( $T_c = 18$  K). Moreover, recent neutron inelastic scattering measurements show the evidence of strong antiferromagnetic fluctuations [8], reconciling LiFeAs with other Fe-based superconductors.

A multigap scenario is suggested by the presence of five different sheets in the Fermi surface [9]: two electron pockets are centered near the  $M$ -point of the Brillouin zone and three hole pockets around the  $\Gamma$ -point. Despite the Fermi surface showing five different sheets, according to our electronic structure calculations the fifth sheet can be disregarded because of its low density of states (see table 1 and

figure 1) and size<sup>3</sup> [10–13]. Consequently, as a starting point, we can model the electronic structure of LiFeAs by using a four-band model [14, 15] with two hole bands (1 and 2) and two electron bands (3 and 4).

In this work we construct a theoretical model to describe the phenomenology of LiFeAs, by using a minimal number of phenomenological parameters in combination with density functional theory (DFT) calculations and the Eliashberg theory of superconductivity. The model is then tested by simulating the temperature dependence of the critical field.

Recently, four different gaps have been observed by ARPES measurements on LiFeAs [17]. Hence, in order to describe the superconductive properties of this compound, a four-band Eliashberg model [14, 15] with  $s_{\pm}$  symmetry [16] can be used.

The experimental gap values [17] have been used to fix the free parameters of the model and, after this,

<sup>3</sup> Electronic structure calculations are done within Kohn–Sham [10] density functional theory in the PBE [11] approximation for the exchange correlation functional and using the experimental lattice structure [5]. Ultrasoft pseudopotentials are used to describe core states, while valence wavefunctions are expanded in planewaves with a 40 Ryd cutoff (400 Ryd for charge expansion). We use the implementation provided by the ESPRESSO package [12]. A coarse grid of  $20 \times 20 \times 16$   $\mathbf{k}$ -points is explicitly calculated and then Fourier interpolated to compute accurate Fermi velocities and plasma frequencies.

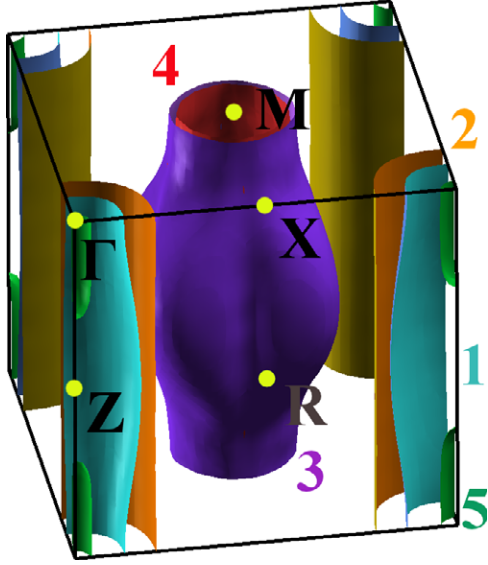


**Figure 1.** Fermi surface of LiFeAs.

the critical temperature and the upper critical magnetic field [18] have been calculated. The final result is a moderately strong coupling regime  $\lambda_{\text{tot}} \sim 1.6\text{--}2.0$  where the total electron–boson coupling must include two different contributions: a purely interband coupling mediated by spin-fluctuations (sf), with  $\lambda_{\text{tot}}^{\text{sf}} \sim 1.5$  and a purely intraband coupling  $\lambda_{11}$ , whose origin will be discussed hereafter. The isotropic values of the gaps at  $T = 8$  K are reported to be  $\Delta_1 = 5.0$  meV,  $\Delta_2 = 2.6$  meV,  $\Delta_3 = 3.6$  meV,  $\Delta_4 = 2.9$  meV. As a first approximation, since just a small anisotropy is observed, we consider only the isotropic part.

The Eliashberg theory [19] generalized to multiband systems has already been successfully used to describe the properties of MgB<sub>2</sub> [20–22] and iron-compounds [23, 24]. A four-band Eliashberg model includes eight coupled equations for the gaps  $\Delta_i(i\omega_n)$  and the renormalization functions  $Z_i(i\omega_n)$ , where  $i$  is the band index (that ranges between 1 and 4) and  $\omega_n$  are the Matsubara frequencies. The imaginary-axis equations are:

$$\omega_n Z_i(i\omega_n) = \omega_n + \pi T \sum_{m,j} \Lambda_{ij}^Z(i\omega_n, i\omega_m) N_j^Z(i\omega_m) + \sum_j [\Gamma_{ij} + \Gamma_{ij}^M] N_j^Z(i\omega_n) \quad (1)$$

$$Z_i(i\omega_n) \Delta_i(i\omega_n) = \pi T \sum_{m,j} [\Lambda_{ij}^\Delta(i\omega_n, i\omega_m) - \mu_{ij}^*(\omega_c)] \times \Theta(\omega_c - |\omega_m|) N_j^\Delta(i\omega_m) + \sum_j [\Gamma_{ij} + \Gamma_{ij}^M] N_j^\Delta(i\omega_n) \quad (2)$$

where  $\Gamma_{ij}$  and  $\Gamma_{ij}^M$  are the nonmagnetic and magnetic impurity scattering rates,  $\Lambda_{ij}^Z(i\omega_n, i\omega_m) = \Lambda_{ij}^{\text{ph}}(i\omega_n, i\omega_m) + \Lambda_{ij}^{\text{sf}}(i\omega_n, i\omega_m)$ ,  $\Lambda_{ij}^\Delta(i\omega_n, i\omega_m) = \Lambda_{ij}^{\text{ph}}(i\omega_n, i\omega_m) - \Lambda_{ij}^{\text{sf}}(i\omega_n, i\omega_m)$ , sf means antiferromagnetic spin-fluctuations and *ph* phonons.

$\Theta(\omega_c - |\omega_m|)$  is the Heaviside function and  $\omega_c$  is a cutoff energy. In particular,  $\Lambda_{ij}^{\text{ph,sf}}(i\omega_n, i\omega_m) = 2 \int_0^{+\infty} d\Omega \Omega$

**Table 1.** Fermi surface resolved Kohn–Sham properties (see footnote 1): The Fermi density of states ( $N(0)$ ) is given in states/spin/eV, the Fermi velocities ( $v_F$ ) in  $10^5$  m s<sup>-1</sup>, and plasma frequencies ( $\omega_p$ ) in eV. *ab* is the in-plane and *c* is the out-of-plane direction of the Fermi velocities and the diagonals of the plasma tensor [13].

FS	$N(0)$	$v_F^{\parallel ab}$	$v_F^{\parallel c}$	$\omega_p^{\parallel ab}$	$\omega_p^{\parallel c}$
1	0.556	1.157	0.207	1.131	0.202
2	0.646	1.382	0.032	1.455	0.034
3	0.616	1.535	0.865	1.581	0.890
4	0.370	2.014	0.459	1.161	0.365
5	0.039	2.454	1.227	0.639	0.319
TOT	2.228	1.523	0.529	2.980	1.035

$\frac{\alpha_{ij}^2 F^{\text{ph,sf}}(\Omega)}{(\omega_n - \omega_m)^2 + \Omega^2}$ ,  $\mu_{ij}^*(\omega_c)$  are the elements of the  $4 \times 4$  Coulomb pseudopotential matrix and, finally,

$$N_j^\Delta(i\omega_m) = \Delta_j(i\omega_m) \left[ \sqrt{\omega_m^2 + \Delta_j^2(i\omega_m)} \right]^{-1},$$

$$N_j^Z(i\omega_m) = \omega_m \left[ \sqrt{\omega_m^2 + \Delta_j^2(i\omega_m)} \right]^{-1}.$$

The electron–boson coupling constants are defined as

$$\lambda_{ij}^{\text{ph,sf}} = 2 \int_0^{+\infty} d\Omega \frac{\alpha_{ij}^2 F^{\text{ph,sf}}(\Omega)}{\Omega}. \quad (3)$$

The solution of equations (1) and (2) requires a huge number of input parameters (32 functions and 16 constants); nevertheless, some of these are interdependent, others may be extracted from experiments and still others fixed by appropriate approximations.

At the beginning we fixed the same conditions that have been used for many other pnictides, as shown in [16], and we assumed that: (i) the total electron–phonon coupling constant is small and mostly intraband [25]; (ii) antiferromagnetic spin-fluctuations mainly provide interband coupling [3, 23]. To account for these assumptions in the simplest way (as has already been done for other iron-compounds with good results) we should take:  $\lambda_{ii}^{\text{ph}} = \lambda_{ij}^{\text{ph}} = 0$ ,  $\mu_{ii}^*(\omega_c) = \mu_{ij}^*(\omega_c) = 0$  i.e. the electron–phonon coupling constant and the Coulomb pseudopotential compensate each other, in first approximation, and  $\lambda_{ii}^{\text{sf}} = 0$ , i.e. SF produce only interband coupling [23]. However, within these assumptions, we were not able to reproduce the gap values of LiFeAs, and in particular the high value of  $\Delta_1$ , the best results obtained are reported in the second row of table 2.

In order to solve this problem it is necessary to introduce at least an intraband coupling in the first band, then  $\lambda_{11} \neq 0$ .

The final matrix of the electron–boson coupling constants becomes

$$\lambda_{ij} = \begin{pmatrix} \lambda_{11} & 0 & \lambda_{13} & \lambda_{14} \\ 0 & 0 & \lambda_{23} & \lambda_{24} \\ \lambda_{31} = \lambda_{13} \nu_{13} & \lambda_{32} = \lambda_{23} \nu_{23} & 0 & 0 \\ \lambda_{41} = \lambda_{14} \nu_{14} & \lambda_{42} = \lambda_{24} \nu_{24} & 0 & 0 \end{pmatrix} \quad (4)$$

**Table 2.** The first row shows the experimental data. The second row concerns the pure interband case ( $\lambda_{ii} = 0$ ) while the last three include an intraband term ( $\lambda_{11} \neq 0$ ). A very large value appears in the first case (the third row), a smaller one if the phonon spectral function  $G(\Omega)$  (fourth row) or the electron–phonon spectral function  $\alpha^2 F(\Omega)$  (fifth row) are considered. The critical temperatures are given in K and the gap values in meV.

	$\lambda_{11}$	$\lambda_{\text{tot}}$	$\lambda_{13}$	$\lambda_{23}$	$\lambda_{14}$	$\lambda_{24}$	$\Delta_1$	$\Delta_2$	$\Delta_3$	$\Delta_4$	$T_c$
Ex.	—	—	—	—	—	—	5.0	2.6	3.6	2.9	18.0
sf	0.00	1.80	1.78	0.66	0.45	0.52	3.7	2.6	3.6	2.9	15.9
sf, ?	2.10	2.00	1.15	0.80	0.45	0.30	5.0	2.6	3.6	2.9	18.6
sf, ph (1)	0.86	1.62	1.06	0.79	0.42	0.30	5.1	2.6	3.7	2.9	20.0
sf, ph (2)	0.90	1.63	1.15	0.80	0.45	0.30	5.0	2.6	3.6	2.9	20.1

where  $v_{ij} = N_i(0)/N_j(0)$  and  $N_i(0)$  is the normal density of states at the Fermi level for the  $i$ th band ( $i = 1, 2, 3, 4$ ). We chose spectral functions with Lorentzian shape i.e:

$$\alpha_{ij}^2 F_{ij}(\Omega) = C_{ij} \{L(\Omega + \Omega_{ij}, Y_{ij}) - L(\Omega - \Omega_{ij}, Y_{ij})\} \quad (5)$$

where  $L(\Omega \pm \Omega_{ij}, Y_{ij}) = \frac{1}{(\Omega \pm \Omega_{ij})^2 + Y_{ij}^2}$  and  $C_{ij}$  are normalization constants, necessary to obtain the proper values of  $\lambda_{ij}$  while  $\Omega_{ij}$  and  $Y_{ij}$  are the peak energies and half-widths of the Lorentzian functions, respectively [23]. In all the calculations we set  $\Omega_{ij} = \Omega_{ij}^{\text{sf}} = \Omega_0^{\text{sf}} = 8$  meV [8], and  $Y_{ij} = Y_{ij}^{\text{sf}} = \Omega_{ij}^{\text{sf}}/2$  [26]. The cutoff energy is  $\omega_c = 18 \Omega_0^{\text{sf}}$  and the maximum quasiparticle energy is  $\omega_{\text{max}} = 21 \Omega_0^{\text{sf}}$ . We put  $\Gamma_{ij} = \Gamma_{ij}^M = 0$  because the ARPES measurement are on very good single crystals of LiFeAs [17]. Bandstructure calculations (see table 1) provide information about the factors  $v_{ij}$  that enter the definition of  $\lambda_{ij}$ . The obtained values are  $v_{13} = 0.9019$ ,  $v_{14} = 1.5010$ ,  $v_{23} = 1.0483$ ,  $v_{24} = 1.7447$ .

After these considerations the free parameters are reduced to the five coupling constants  $\lambda_{13}$ ,  $\lambda_{23}$ ,  $\lambda_{14}$ ,  $\lambda_{24}$  and  $\lambda_{11}$ . First of all we solved the imaginary-axis Eliashberg equations (1) and (2) (actually we continued them analytically on the real-axis by using the approximants Padè technique) and we fixed the free parameters in order to reproduce the gap values at low temperature.

The large number of free parameters (five) may suggest that it is possible to find different sets that produce the same results. It is not so; as a matter of fact the predominantly interband character of the model drastically reduces the number of possible choices.

At the beginning, in order to have the fewest number of free parameters, we set  $\Omega_{11}$  to be the same as the antiferromagnetic SF (even if the intraband coupling cannot be mediated by SF). In this case (see the third row of table 2) the value of  $\lambda_{11}$  is very large. We add only  $\lambda_{11}$  because only band 1 has a low Fermi energy and only in this band does the Migdal’s theorem break down. The effect of the vertex corrections [27, 28] can be simulated by an effective coupling that is bigger than real coupling [29, 30]. Certainly in bands 2, 3 and 4, the phonon couplings are very small and therefore we have not considered the possibility to have  $\lambda_{22}$ ,  $\lambda_{33}$ ,  $\lambda_{44} \neq 0$  and also, in a previous paper, we have demonstrated that, in these systems, the effect of a small phononic intraband coupling is negligible [23].

Then we considered for  $\Omega_{11}$  the typical phonon energies [7]. In this case (as reported in the fourth and fifth

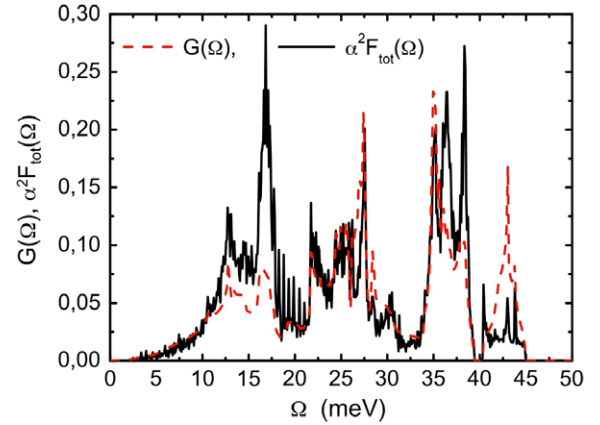


**Figure 2.** The calculated phononic density of states  $G(\Omega)$  (red dashed line) and the calculated total electron–phonon spectral function  $\alpha^2 F_{\text{tot}}(\Omega)$  (black solid line).

rows of table 2) the value of  $\lambda_{11}$  is 0.86–0.9, while the antiferromagnetic spin-fluctuations contribution corresponds to a moderately strong coupling regime ( $\lambda_{\text{tot}}^{\text{sf}} \sim 1.5$ ).

In fact, we have solved the Eliashberg equations in two other cases: in the first case we used as  $\alpha_{11}^2 F(\Omega)$  the calculated phonon density of states  $G(\Omega)$  and in the second case we considered the calculated total electron–phonon spectral function  $\alpha^2 F_{\text{tot}}(\Omega)$ , both appropriately scaled. The proper choice is the second one, but this spectral function should, in principle, be different for each band; since the first band shows peculiar characteristics the evaluation of the electron–phonon coupling could be not so reliable. Then we decided to use the phonon spectra and let the coupling be a free parameter. These spectral functions are shown in figure 2.

At this point there are no more free parameters. The critical temperature can be evaluated and it turns out to be very close to the experimental one,  $T_c^{\text{calc}} = 18.6\text{--}20.1$  K.

By solving the real-axis Eliashberg equations we obtained the temperature dependence of the gaps (see figure 3) for the parameter sets reported in the third and fourth rows of table 2.

The multiband Eliashberg model developed above can also be used to explain the experimental data of the temperature dependence of the upper critical magnetic field [18]. For the sake of completeness, we give here the linearized gap equations in the presence of the magnetic field, for a superconductor in the clean limit. In the following,  $v_{Fj}$  is the Fermi velocity of the  $j$ th band, and  $H_{c2}$  is the upper critical

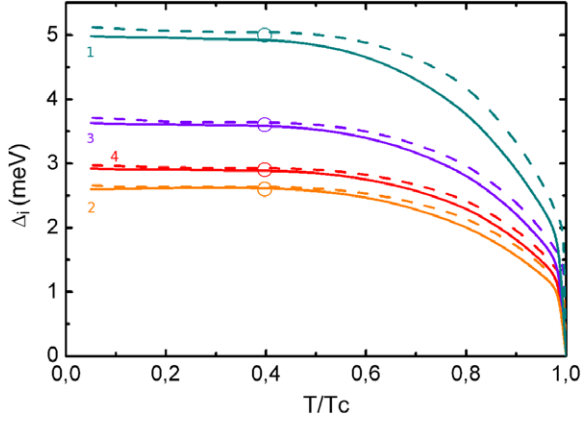


**Figure 3.** Temperature dependence of the absolute gap values (lines) and experimental data (symbols) at 8 K. The dark cyan solid (dashed) line represents the first gap, the orange solid (dashed) line the second one, the violet solid (dashed) line the third and the red solid (dashed) line the fourth, calculated with the parameters of the fourth (third) row of table 2.

field:

$$\omega_n Z_i(i\omega_n) = \omega_n + \pi T \sum_{m,j} \Lambda_{ij}^Z(i\omega_n - i\omega_m) \text{sign}(\omega_m) \quad (6)$$

$$Z_i(i\omega_n) \Delta_i(i\omega_n) = \pi T \sum_{m,j} \left[ \Lambda_{ij}^\Delta(i\omega_n - i\omega_m) - \mu_{ij}^*(\omega_c) \right] \times \theta(|\omega_c| - \omega_m) \chi_j(i\omega_m) Z_j(i\omega_m) \Delta_j(i\omega_m) \quad (7)$$

$$\chi_j(i\omega_m) = \frac{2}{\sqrt{\beta_j}} \int_0^{+\infty} dq \exp(-q^2) \times \tan^{-1} \left[ \frac{q\sqrt{\beta_j}}{|\omega_m Z_j(i\omega_m)| + i\mu_B H_{c2} \text{sign}(\omega_m)} \right].$$

Here  $\beta_j = \pi H_{c2} v_{Fj}^2 / (2\Phi_0)$  and  $\Phi_0$  is the unit of magnetic flux. In these equations the four bare Fermi velocities  $v_{Fj}$  [31] are the input parameters. As the first band shows that peculiar characteristics even in the calculation of the Fermi velocity can be present in some corrections, we decided to let the first Fermi velocities be free parameters and we chose them to find the best fit of the experimental data [18] while the other values have been fixed to the values reported in table 1. Then  $v_{F1}$ , in each case, is the only free parameter. The obtained values are:  $v_{F1}^{\parallel c} = 2.28 \times 10^5 \text{ m s}^{-1}$  and  $v_{F1}^{\parallel ab} = 1.74 \times 10^5 \text{ m s}^{-1}$ , in the phonon case and  $v_{F1}^{\parallel c} = 2.79 \times 10^5 \text{ m s}^{-1}$  and  $v_{F1}^{\parallel ab} = 2.14 \times 10^5 \text{ m s}^{-1}$ , if the spin-fluctuation spectral function is considered. Figure 4 shows the experimental data and the best theoretical curves (solid and dashed lines) obtained by solving the Eliashberg equations within the model discussed above. As can be seen, the results obtained in the two considered cases are almost indistinguishable and in very good agreement with the experimental data. In figure 4 we also show the curves calculated with  $v_{F1}$  taken from table 1 when  $\lambda_{11} \neq 0$  (the fourth case in table 2, dotted line olive and navy) and when  $\lambda_{11} = 0$  (the first case in table 2, dashed-dotted line magenta and pink). In both situations there is no agreement with the experimental data. The curves calculated in absence

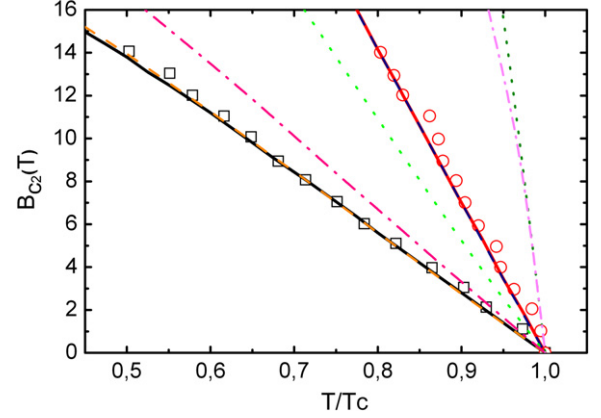


**Figure 4.** Experimental temperature dependence of the upper critical field (symbols), and the relevant fitting curves (lines) obtained by solving the Eliashberg equations in the magnetic field. Red circles and a solid red (dashed dark blue) line stand for  $H_{\parallel c}$ , black square symbols and a solid black (dashed orange) line stand for  $H_{\parallel ab}$  calculated with the parameters of the fourth (third) row of table 2. The dotted olive ( $H_{\parallel c}$ ), navy ( $H_{\parallel ab}$ ), dashed-dotted magenta ( $H_{\parallel c}$ ) and pink ( $H_{\parallel ab}$ ) lines are, respectively, the fourth and first cases of table 2 but where  $v_{F1}$  is not a free parameter but is taken from table 1.

of the term  $\lambda_{11}$  do not agree with the experimental data so we deduce that the higher value of  $v_{F1}^{\parallel ab,c}$  is not produced by the presence of an intraband term ( $\lambda_{11} \neq 0$ ) but, probably, by the peculiar characteristics of band 1. However one must consider the fact that the Eliashberg equations are derived by assuming Migdal's theorem. In presence of an anomalous band dispersion as for band 1, the theory may partially break down. Allowing  $v_{F1}^{\parallel ab,c}$  as a free parameter implicitly implies that we are 'phenomenologically' going beyond the first order contributions (i.e. now we cannot neglect the effects of the vertex corrections in band 1). The break down of Migdal's theorem leads to the use of effective values of  $\lambda_{11}$  and  $v_{F1}$  different from the real value because the framework of the theory is partially inadequate.

To summarize we have constructed a phenomenological model of superconductivity for LiFeAs able to describe its critical temperature, the multigap structure measured by Umezawa and coworkers in [17] and other experimental observations. However this process was not straightforward. To be able to conjugate a spin-fluctuation dominated pairing with the experimental gap structure we have been forced to introduce an intraband coupling that acts only on the first band. The presence of a phononic, purely intraband term seems to indicate an intrinsic incompatibility between the structure of the superconducting gaps as measured by Umezawa and coworkers in [17] and a purely spin-fluctuation mediated pairing. A possible explanation may be linked to the very low Fermi energy of the band for which vertex corrections [27, 28] to the usual Migdal-Eliashberg theory may be relevant, and are expected to increase the strength of the phononic pairing [29, 30].

In conclusion, our calculations show that LiFeAs presents peculiar features with respect to other iron-compounds and it

cannot be explained within the framework of a pure interband spin-fluctuation mediated superconductivity.

## References

- [1] Kamihara Y, Watanabe T, Hirano M and Hosono H 2008 *J. Am. Chem. Soc.* **130** 3296
- [2] Stewart G R 2011 *Rev. Mod. Phys.* **83** 1589
- [3] Hirschfeld P J, Korshunov M M and Mazin I I 2011 *Rep. Prog. Phys.* **74** 124508
- [4] Johnston D C 2010 *Adv. Phys.* **59** 803
- [5] Tapp J H, Tang Z, Lv B, Sasmal K, Lorenz B, Chu P C W and Guloy A M 2008 *Phys. Rev. B* **78** 060505
- [6] Borisenko S V *et al* 2010 *Phys. Rev. Lett.* **105** 067002
- [7] Huang G Q, Xing Z W and Xing D Y 2010 *Phys. Rev. B* **82** 014511
- [8] Taylor E A, Pitcher M J, Ewings R A, Perring T G, Clarke S J and Boothroyd A T 2011 *Phys. Rev. B* **83** 220514R
- [9] Singh D J 2008 *Phys. Rev. B* **78** 094511
- [10] Kohn W and Sham L J 1965 *Phys. Rev.* **140** A1133
- [11] Perdew J P, Burke K and Ernzerhof M 1996 *Phys. Rev. Lett.* **77** 3865
- [12] Giannozzi P *et al* 2009 *J. Phys.: Condens. Matter* **21** 395502
- [13] Golubov A A, Brinkman A, Dolgov O V, Kortus J and Jepsen O 2002 *Phys. Rev. B* **66** 054524
- [14] Benfatto L, Cappelluti E and Castellani C 2009 *Phys. Rev. B* **80** 214522
- [15] Popovich P, Boris A V, Dolgov O V, Golubov A A, Sun D L, Lin C T, Kremer R K and Keimer B 2010 *Phys. Rev. Lett.* **105** 027003
- [16] Mazin I I, Singh D J, Johannes M D and Du M H 2008 *Phys. Rev. Lett.* **101** 057003
- [17] Umezawa K *et al* 2012 *Phys. Rev. Lett.* **108** 037002
- [18] Kasahara S, Hashimoto K, Ikeda H, Terashima T, Matsuda Y and Shibauchi T 2012 *Phys. Rev. B* **85** 060503
- [19] Eliashberg G M 1960 *Sov. Phys.—JETP* **11** 696
- [20] Shulga S V, Drechsler S-L, Fuchs G and Müller K-H 1998 *Phys. Rev. Lett.* **80** 1730
- [21] Ummarino G A, Gonnelli R S, Massidda S and Bianconi A 2004 *Physica C* **407** 12
- [22] Nicol E J and Carbotte J P 2005 *Phys. Rev. B* **71** 054501
- [23] Ummarino G A, Tortello M, Daghero D and Gonnelli R S 2009 *Phys. Rev. B* **80** 172503
- [24] Ummarino G A, Daghero D, Tortello M and Gonnelli R S 2011 *J. Supercond. Novel Magn.* **24** 247
- [25] Boeri L, Calandra M, Mazin I I, Dolgov O V and Mauri F 2010 *Phys. Rev. B* **82** 020506R
- [26] Inosov D S *et al* 2010 *Nature Phys.* **6** 178–81
- [27] Pietronero L, Strässler S and Grimaldi C 1995 *Phys. Rev. B* **52** 10516
- [28] Grimaldi C, Pietronero L and Strässler S 1995 *Phys. Rev. B* **52** 10530
- [29] Paci P, Cappelluti E, Grimaldi C and Pietronero L 2001 *Phys. Rev. B* **65** 012512
- [30] Ummarino G A and Gonnelli R S 1997 *Phys. Rev. B* **56** R14279
- [31] Suderow H, Tissen V G, Brison J P, Martínez J L, Vieira S, Lejay P, Lee S and Tajima S 2004 *Phys. Rev. B* **70** 134518